Journal of Fluids and Structures 18 (2003) 387–403

JOURNAL OF FLUIDS AND STRUCTURES

www.elsevier.nl/locate/jnlabr/yjfls

Numerical simulation of turbulent wake flows behind two side-by-side cylinders

Li Chen[a], J.Y. Tu[b], G.H. Yeoh[c,*]

[a] *Maritime Platforms Division, DSTO, P.O. Box 4331, Victoria 3001, Australia*
[b] *School of Aerospace, Mechanical and Manufacturing Engineering, RMIT University, Victoria 3083, Australia*
[c] *Australian Nuclear Science and Technology Organisation (ANSTO), PMB 1, Menai, NSW 2234, Australia*

Abstract

The formation and the convection of vortices behind two side-by-side cylinders are investigated using the large-eddy simulation (LES) model. Solution to the three-dimensional Navier–Stokes governing equations is obtained using a finite volume method with an unstructured mesh arrangement with hexahedral elements. The focus of the present investigation is to predict the wake dynamics at Reynolds numbers $Re = 750$ at two different cylinder spacings: large ratio $T/d = 3$ and intermediate ratio $T/d = 1.7$. The LES results revealed that for $T/d = 3$, the formation of symmetrical wakes behind the cylinders was observed. Two distinct vortex streets propagated downstream. However, for $T/d = 1.7$, owing to the close proximity of the two cylinders, the gap flow between the cylinders was deflected, forming one narrow and one wide wake behind the cylinders. It was also succinctly revealed that the gap flow deflection has a tendency to "flip", changing over from one side to another by being deflected upwards at a specific instance and downwards at later time. Qualitatively, the phenomenological predictions are in accordance with experimental observations.

1. Introduction

Flow over bluff bodies is widely encountered in many practical applications. A moving maritime platform, a heat exchanger with crossflow fluid passages to periodically disrupt the flow, air-flow around buildings, and combustors with flame holders are just some of these fundamental and challenging fluid mechanics problems. Concerning heat exchanger design, Liou et al. (1995) succinctly demonstrated through their experiments that an oscillating flow resulting from spanwise turbulent vortices behind a circular cylinder near a heated wall can significantly enhance the heat transfer along the wall due to periodically sweeping movements of the thermal boundary layer. In sustaining and maintaining the safe operations of maritime platforms, and heat exchangers in industrial boilers and nuclear reactors, a thorough understanding of the vortex structures could also assist in alleviating problems associated with flow-induced vibration and noise that may compromise the structural integrity (Goyder, 2002).

Flow over a cylinder has been studied extensively. It exhibits vastly different behaviour as the Reynolds number, based on the free-stream velocity, cylinder diameter, and kinematic viscosity, increases from zero to large values. Steady laminar flow exists at Reynolds number up to approximately $Re \sim 40$ with a pair of symmetric counter-rotating vortices behind the cylinder at $Re > 5$. Increasing further the Reynolds number, the laminar vortex shedding, also known as the Karman vortex street, is observed at Reynolds number up to about $Re \sim 190$. The next regime, indicated by Williamson (1996) as the regime of mode A instability, lies in the range of Reynolds numbers between 190 and 260. Barkley and Henderson (1996) performed a three-dimensional Floquet stability analysis of the cylinder wake and suggested that the

*Corresponding author. Tel.: +61-2-9717-3817; fax: +61-2-9717-9263.
E-mail address: guan.yeoh@ansto.gov.au (G.H. Yeoh).

0889-9746/$ - see front matter © 2003 Elsevier Ltd. All rights reserved.
doi:10.1016/j.jfluidstructs.2003.08.005

critical value of the Reynolds number of $Re = 188.5 \pm 1.0$ for the onset of this regime. At a Reynolds number of approximately 260, the flow experiences transition to finer scale three-dimensionality, known as mode B instability, with spanwise characteristic length of around one cylinder diameter. With increasing Reynolds number, the three-dimensional cylinder wake becomes more chaotic. The shear layers separating from the cylinder become unstable at Reynolds number at about 1200. Prasad and Williamson (1996) highlighted that this critical value of the Reynolds number varies from 300 to 3000.

In the current investigation, we are interested in the problem of flow interference when two cylinders are placed side-by-side in a steady current. Zdravkovich (1977, 1987) observed that when more than one body is placed in a fluid flow, the resulting forces and vortex shedding pattern may be completely different from those found at the same Reynolds number. A variety of flow patterns characterized by the behaviour of the wake region may be discerned as the spacing between two circular cylinders is changed.

Fig. 1 illustrates the schematic arrangement of a two cylinder side-by-side configuration. The flow behaviour is characterized by the ratio of the T/d where T is the centre–centre cylinder spacing and d is the cylinder diameter. Experimental studies by Williamson (1985) and Kim and Durbin (1988) have shown that varying T/d resulted in a variety of flow patterns, which are represented by the flow behaviours in the wake formation region. For a relatively large spacing, $T/d > 2$, two distinct coherent structures of vortex streets are observed. These two vortex streets are strongly coupled, with a definite phase relationship. Spivac (1946) measured a single frequency for $T/d > 2$. This frequency was further established to have the same frequency measured in a single cylinder wake flow. It means that the phenomenological description of the wake dynamics behind a circular cylinder may still hold for two cylinders arranged side-by-side with each other for $T/d > 2$.

Ishigai et al. (1972) performed a flow visualization study on the flow behind two side-by-side cylinders using a Schlieren optical method and observed a remarkably symmetric vortex formation and shedding for $T/d = 2.5$ and 3.0 and Reynolds number ranging between 100 and 200. Williamson (1985) further demonstrated that the two vortex streets have a tendency of being either in phase (anti-symmetric vortex formation) or in antiphase (symmetric vortex formation). It was seen that the in-phase vortex streets eventually converged and merged downstream to form a single street while the in antiphase streets remained distinct farther downstream. He observed a predominant antiphase vortex shedding for T/d between 2 and 6. However, current numerical investigation to further elucidate the predominance of

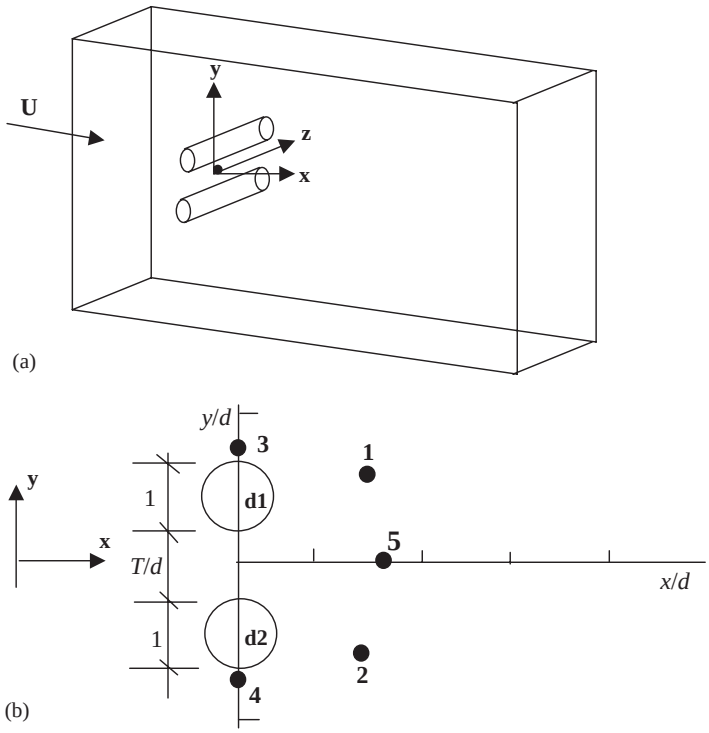

Fig. 1. Schematic drawing of two side-by-side cylinders: (a) three-dimensional perspective and (b) side view and data recording locations.

the symmetric vortex shedding over the anti-symmetric shedding and to determine any possible triggering mechanisms that may cause the transition of the two vortex streets from the in-antiphase to the in-phase mode.

At intermediate cylinder spacing, $1.2 < T/d < 2.0$, instead of two distinct vortex streets observed for the large cylinder spacing, the interaction between the wakes associated within the two cylinders intensifies; the gap flow between the cylinders is deflected, forming one narrow wake and the other a wide wake. Ishigai et al. (1972) ascribed the gap flow deflection to the *Coanda* effect. Contrarily, Bearman and Wadcock (1973) measured different base pressures behind two side-by-side flat plates and they argued that the gap flow deflection was not caused by the boundary layer separation; instead, it was due to the near-wake phenomenon. Their argument was further supported by Williamson (1985) flow visualization, which showed a deflected gap flow behind two side-by-side flat plates. It was found that the vortex frequency associated with the narrow wake approximately triples that for the wide wake (Bearman and Wadcock, 1973; Sumner et al., 1998). The deflected gap flow may change over intermittently from one side to another and is actually bi-stable. It was found by Kim and Durbin (1988) that the bi-stability is nominally independent of the Reynolds number. Recently, Xu et al. (2003) presented a more detailed study on this intermediate spacing. They found that at the spacing $T/d < 1.6$, the formation of the two vortex streets is dependent on the Reynolds number. They also confirmed that two dominant frequencies had a ratio of 3 when two streets existed. The physical mechanisms behind the formation and stability of a narrow and a wide wake and its associated "flipping" phenomenon remain unexplained. In addressing these issues, possible mechanisms that trigger the changeover of the gap flow deflection from one side to another, the reason of the dominant frequency in the narrow wake being triple of that in the wide wake and the evolution of both wakes at downstream are comprehensively studied here.

We are interested in investigating the turbulent wake flow behind two side-by-side cylinders for a Reynolds number of 750 at two T/d ratios of 1.7 and 3. Meneghini et al. (2001) recently performed a two-dimensional finite element study on the flow past two side-by-side cylinders at a Reynolds number of 200. Numerical studies on various T/d ratios were investigated. An earlier study of a two-dimensional investigation by Slaouti and Stansby (1992), at a similar Reynolds number, of wake dynamics behind two circular cylinders using the discrete vortex method including viscous diffusion, modelled by the random walk method, is also noted. As mentioned earlier, we can infer from above that their numerical simulations for the flow Reynolds number studied still lies within the laminar vortex shedding regime. Also, since we are focusing on a flow Reynolds number of 750, the wake being more chaotic, a two-dimensional numerical investigation is deemed insufficient to resolve the finer scale of the three-dimensionality phenomenon.

The simulation of large coherent structures in the turbulent wake flow behind the cylinders is extremely difficult because of the wide-range spectrum of scales. For the turbulent characteristics in the wake region, stochastic three-dimensional turbulent fluctuations are superimposed on the periodic vortex-shedding motion. Majumdar and Rodi (1985) have demonstrated that the widely used Reynolds-averaged Navier–Stokes (RANS) equations based on the standard two-equation turbulence models ($\kappa-\varepsilon$ and $\kappa-l$) are incapable of accurately predicting the vortex-shedding behaviour. The problem with these models in stagnation flows is well known. This is because the turbulent energy production in this flow is attributed by the normal stresses (not shear stresses) and these cannot be simulated correctly with an isotropic eddy-viscosity model, leading to excessive energy production. Rodi (1993) reviewed the application of the models and concluded the general superiority of Reynolds stress model (RSM) over the two-equation models. Nevertheless, the large-eddy simulation of turbulent flows based on the Smagorinsky–Lilly subgrid-scale (SGS) turbulence model is shown to yield far more realistic flow results than those obtained by traditional two-equation turbulence models due to Tutar et al. (1998) or RSM. Based on Rodi et al. (1997) compiled results from the workshop and evaluation of the state-of-the-art LES approach to complex flows, they found that the LES approach was highly recommended because of its ability to resolve the unsteady large-scale turbulent motion. The numerical results generated through the LES model can provide useful turbulent statistics of the cyclic formation of the vortices downstream. It is also concluded that LES-based simulations are not overly expensive in terms of computing time when compared with traditional turbulence model simulations.

The present work therefore deals with a three-dimensional numerical investigation of a turbulent flow past a configuration of two side-by-side circulars using LES to resolve the flow-induced wake turbulence. The motivation of this work is driven by the recent experimental observations performed by Zhou et al. (2001) in the water tunnel facility. They had visualized the complex formation of the dynamics for low and high Reynolds numbers for the side-by-side cylinder arrangement with various T/d ratios, which allows for direct comparison with the current flow predictions. The main objectives of this work are:

(i) to validate our phenomenological predictions with the flow visualization experimental results of Zhou (2002);
(ii) to elucidate the aforementioned issues in the different wake flow behaviour behind the cylinders for two T/d ratios of 1.7 and 3 and
(iii) to gain a more fundamental understanding of the physical processes within the wake formation region at these two ratios for the flow Reynolds number of 750.

2. Theoretical background

2.1. Governing equations

The flow variables are decomposed into a large-scale (or resolved) part that can be solved explicitly and a small-scale part that is modelled with an SGS model. The filtering operation proceeds according to

$$\bar{\phi} = \int_{\Delta} \phi(x_i') G_{\Delta}(x_i, x_i')\, \mathrm{d}x_i', \quad x_i' \in \Delta, \tag{1}$$

$$G_{\Delta}(x_i, x_i') = \begin{cases} 1/\Delta & \text{for } x_i' \in \Delta, \\ 0 & \text{otherwise}, \end{cases} \tag{2}$$

where G is a filter function, decomposing a variable ϕ into a large-scale component $\bar{\phi}$ and a SGS component ϕ', which accounts for the scales not resolved by the filter width Δ:

$$\phi = \bar{\phi} + \phi'. \tag{3}$$

The filtered forms of the incompressible conservation of mass and momentum with an SGS model can be respectively written as

$$\frac{\partial \bar{u}}{\partial x} + \frac{\partial \bar{v}}{\partial y} + \frac{\partial \bar{w}}{\partial z} = 0, \tag{4}$$

$$\frac{\partial \bar{u}}{\partial t} + \frac{\partial \bar{u}\bar{u}}{\partial x} + \frac{\partial \bar{u}\bar{v}}{\partial y} + \frac{\partial \bar{u}\bar{w}}{\partial z} = -\frac{1}{\rho}\frac{\partial \bar{p}}{\partial x} + \nu\left(\frac{\partial^2 \bar{u}}{\partial x^2} + \frac{\partial^2 \bar{u}}{\partial y^2} + \frac{\partial^2 \bar{u}}{\partial z^2}\right) - \left(\frac{\partial \tau_{s_{xx}}}{\partial x} + \frac{\partial \tau_{s_{xy}}}{\partial y} + \frac{\partial \tau_{s_{xz}}}{\partial z}\right), \tag{5}$$

$$\frac{\partial \bar{v}}{\partial t} + \frac{\partial \bar{v}\bar{u}}{\partial x} + \frac{\partial \bar{v}\bar{v}}{\partial y} + \frac{\partial \bar{v}\bar{w}}{\partial z} = -\frac{1}{\rho}\frac{\partial \bar{p}}{\partial y} + \nu\left(\frac{\partial^2 \bar{v}}{\partial x^2} + \frac{\partial^2 \bar{v}}{\partial y^2} + \frac{\partial^2 \bar{v}}{\partial z^2}\right) - \left(\frac{\partial \tau_{s_{yx}}}{\partial x} + \frac{\partial \tau_{s_{yy}}}{\partial y} + \frac{\partial \tau_{s_{yz}}}{\partial z}\right), \tag{6}$$

$$\frac{\partial \bar{w}}{\partial t} + \frac{\partial \bar{w}\bar{u}}{\partial x} + \frac{\partial \bar{w}\bar{v}}{\partial y} + \frac{\partial \bar{w}\bar{w}}{\partial z} = -\frac{1}{\rho}\frac{\partial \bar{p}}{\partial z} + \nu\left(\frac{\partial^2 \bar{w}}{\partial x^2} + \frac{\partial^2 \bar{w}}{\partial y^2} + \frac{\partial^2 \bar{w}}{\partial z^2}\right) - \left(\frac{\partial \tau_{s_{zx}}}{\partial x} + \frac{\partial \tau_{s_{zy}}}{\partial y} + \frac{\partial \tau_{s_{zz}}}{\partial z}\right), \tag{7}$$

where $\bar{u}$, $\bar{v}$, $\bar{w}$ and $\bar{p}$ are the filtered velocity components along the Cartesian axes x, y and z and pressure, respectively. The unsolved subgrid turbulent stresses $\tau_{s_{ij}}$ can be modelled as

$$\begin{aligned}
&\tau_{s_{xx}} = (\overline{uu} - \bar{u}\bar{u}) = 2\nu_s \frac{\partial \bar{u}}{\partial x} - \frac{2}{3}\kappa_s, \quad \tau_{s_{yy}} = (\overline{vv} - \bar{v}\bar{v}) = 2\nu_s \frac{\partial \bar{v}}{\partial y} - \frac{2}{3}\kappa_s, \\
&\tau_{s_{zz}} = (\overline{ww} - \bar{w}\bar{w}) = 2\nu_s \frac{\partial \bar{w}}{\partial z} - \frac{2}{3}\kappa_s, \quad \tau_{s_{xy}} = \tau_{s_{xy}} = (\overline{uv} - \bar{u}\bar{v}) = \nu_s\left(\frac{\partial \bar{u}}{\partial y} + \frac{\partial \bar{v}}{\partial x}\right), \\
&\tau_{s_{xz}} = \tau_{s_{zx}} = (\overline{uw} - \bar{u}\bar{w}) \leftrightarrows = \nu_s\left(\frac{\partial \bar{u}}{\partial z} + \frac{\partial \bar{w}}{\partial x}\right), \quad \tau_{s_{yz}} = \tau_{s_{zy}} = (\overline{vw} - \bar{v}\bar{w}) = \nu_s\left(\frac{\partial \bar{v}}{\partial z} + \frac{\partial \bar{w}}{\partial y}\right).
\end{aligned} \tag{8}$$

The subgrid kinematic viscosity, ν_s, and subgrid turbulent kinetic energy, κ_s, are prescribed by the eddy-viscosity model of Smagorinsky–Lilly (Smagorinsky, 1963):

$$\nu_s = l_s^2 |\bar{S}_{ij}|, \bar{S}_{ij} = \left(\frac{\partial \bar{u}_i}{\partial x_j} + \frac{\partial \bar{u}_j}{\partial x_i}\right), |\bar{S}_{ij}| = \sqrt{2\bar{S}_{ij}\bar{S}_{ij}}. \tag{9}$$

Here, l_s is the mixing length for the subgrid scales calculated as

$$l_s = \min(ky, C_s \Delta^{1/3}), \tag{10}$$

where k is a model constant equivalent to 0.42 and y is the distance closest to the wall. The first term in Eq. (10) accounts for the reduction of the subgrid length l_s near solid walls. Based on Piomelli et al. (1988) and Scotti et al. (1993), the Smagorinsky–Lilly constant C_s is usually taken to lie within a range of 0.1–0.13. Since values higher than 0.13 and lower than 0.1 cause excessive damping of the large-scale fluctuations and convergence problem, respectively, we have conservatively prescribed the constant C_s to be 0.1. Tutar et al. (1998) have successfully demonstrated the feasibility of applying the Smagorinsky–Lilly SGS model to investigate flow past a circular cylinder in the subcritical flow regime. In their later work Tutar and Holdø (2000) applied the Smagorinsky–Lilly SGS model to simulate the fluid–cylinder interactions with different modes of oscillatory motion using the finite element approach. The Smagorinsky–Lilly SGS model is therefore employed, which is deemed sufficient to adequately resolve the small scales of wake eddies for the flow Reynolds number of 750.

2.2. Numerical methods

A finite volume method was employed to obtain a solution of the spatially averaged Navier–Stokes equations. An unstructured mesh arrangement with hexahedral elements was adopted to map the flow domain. The flexible use of unstructured elements provided the ease of concentrating the mesh around the cylindrical outer boundaries to better predict the wake dynamics. The coupling between the pressure and velocity fields was achieved using the SIMPLE technique.

The discretization of the convection terms is a potential source of numerical error in LES calculation and is a subject of constant debate. Flux limiting or TVD-type schemes (Jones, 1994), which improve numerical accuracy in Reynolds average calculations considerably, fail for LES calculation unless the resolution is very high (Boris et al., 1992). As with other asymmetric approximations to the convection terms, they introduce damping to the discretized equations that scales with the cell Peclet number. This can remove a large part of the turbulence and even lead to a predicted but unphysical laminarization. It is well known that although central differences are free from "numerical" diffusion, the corresponding solutions can exhibit oscillatory behaviour (Leonard and Mokhtari, 1990). Nevertheless, according to Mittal and Moin (1997), a second-order central difference solution of flow past a cylinder produces better velocity power spectra, when compared to experiments, than the higher-order upwind schemes. Higher-order upwind schemes give rise to large errors in the smallest simulated scales if these are not properly resolved and thus do not seem to offer a prospect of improved accuracy in the LES calculations considered. Breuer (1998) also stressed the important aspect of low-diffusion discretization schemes in the case for turbulent flow past a circular cylinder. His investigation confirmed that second-order or fourth-order central difference schemes are well suited for LES. Therefore, in the present study, all spatial terms are approximated using second-order central differences. An implicit difference scheme was used with the time derivative represented by the second-order accurate backward difference approximation. The overall solution procedure is second-order accurate in both space and time.

2.3. Computational details and boundary conditions

Before proceeding towards generating any meaningful results, some numerical aspects are addressed. In order to account for the essential flow scales, attention is directed towards a careful grid design. Jordan and Ragab (1998) have demonstrated that a two-dimensional simulation overestimates the strength and the shedding frequency while under-predicting the formation region. Resolving the correct base pressure and Strouhal number is therefore an essential prerequisite of the three-dimensional computation.

Adequate resolution of the streamwise near-wake structures, which are spanwise periodic, is another major concern in the three-dimensional simulation. A sensitivity analysis was performed to ascertain the influence of grid distribution along the spanwise direction. Calculations were performed employing 6 grid points, yielding a length scale of 3 diameters, and 20 grid points, yielding a length scale of 3.6 diameters, to resolve the large-scale eddies. The former gave around two grid points for each of the three eddies while the latter provided a minimum of four spanwise points for each of the three eddies. Fig. 2 presents the instantaneous magnitude of vorticity for the two grid distributions at T/d ratio of 3. The results revealed little difference in the overall flow behaviour on the formation of wake structures past the two circular cylinders between the coarser and finer spanwise distributions. In view of quicker computations and optimizing computational resources, a length scale of 3 diameters, using 6 grid points along the spanwise direction, was deemed sufficient to adequately capture the large-scale wake eddies. Fig. 3 shows a typical snapshot of the iso-surfaces of the instantaneous spanwise and streamwise vorticities, which demonstrates the three-dimensional character of the side-by-side cylinder near-wake structures, as clearly represented by the fine-scale streamwise vortex structures, termed as "vortex loops" and "streamwise vortex pairs".

Along the streamwise and vertical directions, the computational boundaries were set at 22 and 15 diameters, respectively. The upstream boundary was located 7 diameters away from the centreline of the two circular cylinders. The inlet boundary condition was determined from experiment, i.e., the measured turbulent intensity I equal to 0.4%. The value of turbulence fluctuation on individual mean velocity was calculated based on the specified turbulence intensity with a Gaussian random number. The vertical distance adopted was also found sufficient to accommodate the free-stream boundary condition at the top and bottom boundaries of the computational domain, i.e., $u = \{u_\infty, 0, 0\}$. The exit boundary was extended to 15 diameters from the centreline of the cylinders to exclude the influence of outlet boundary conditions on the formation region. A nondiffusion boundary condition was employed at the outer boundary, which ensured the flow at the outer boundary did not affect the flow upstream. A no-slip boundary condition was applied at the inner boundaries representing the cylinder surfaces. To complete the kinematic definition, we applied periodic end conditions in the spanwise direction.

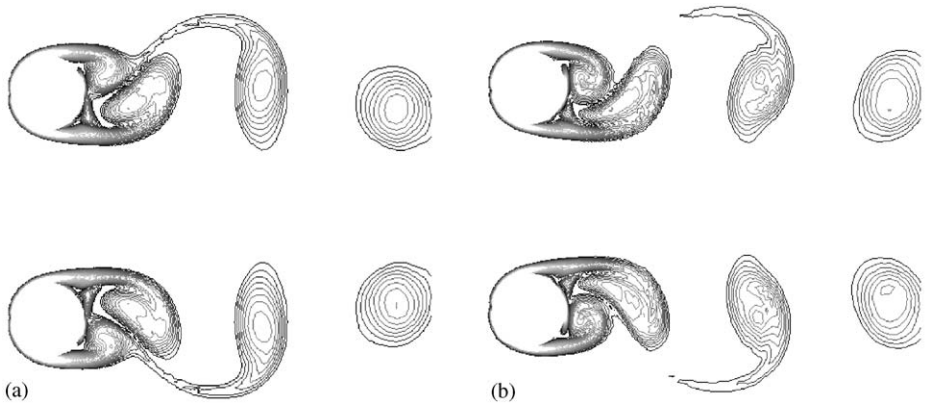

Fig. 2. Effect of mesh size on the instantaneous magnitude of vorticity ($|\omega| = 2-50$): (a) for 6 grid points and (b) for 20 grid points in the spanwise direction.

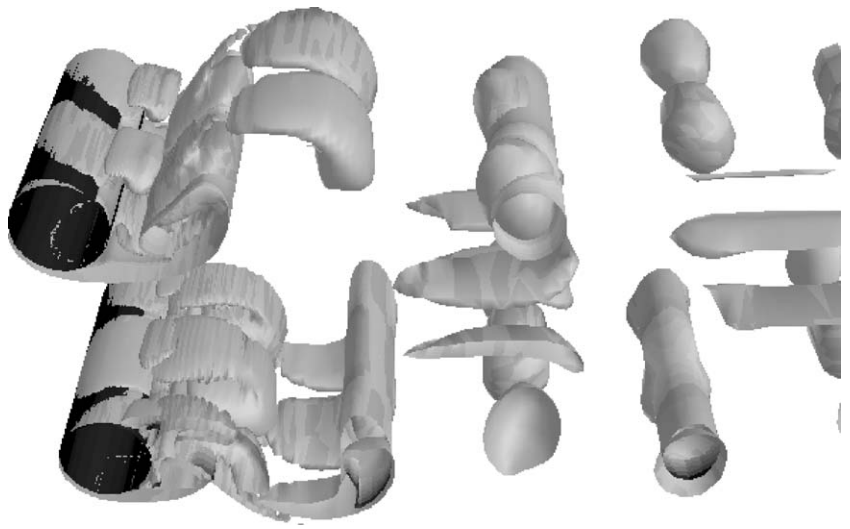

Fig. 3. A three-dimensional perspective view of the vortex shedding structures behind the side-by-side cylinders: the iso-surfaces of spanwise and streamwise vorticity ($|\omega_z| = 20$ and $|\omega_x| = 1$).

A nonuniform fine mesh was used to provide a better description of the boundary layer. The first point condition near the wall, in the wall unit of y^+, ensured that it was less than 1. A substantial amount of grid points were also accommodated in the vicinity of the two cylinders to resolve the near-wake region. The final grid system for the two side-by-side circular cylinder configuration comprised of a total of 630 000 grid points.

3. Results and discussion

3.1. Symmetrical formation of vortex streets at large cylinder spacing

Fig. 4 shows the predicted contours of instantaneous spanwise vorticity and the formation of laser-illuminated dye wake structures recently observed by Zhou (2002) in experiments for flow past two side-by-side cylinders. The flow visualization experiments were performed in a water tunnel with a square working section with various transverse spacing ratios T/d covering a range of low and high Reynolds numbers. More details regarding the experimental configuration can be found in their recent publication (Zhou et al., 2001).

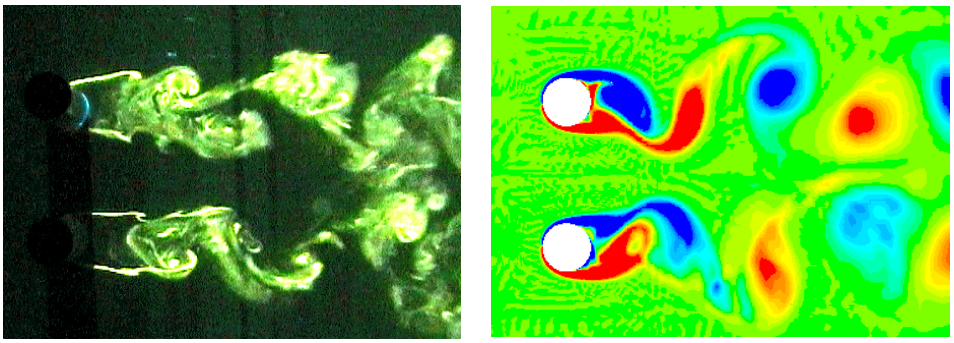

(a) (b)

Fig. 4. Comparison of vortex structures—the contours of instantaneous spanwise vorticity between $|\omega_z| = 20$: (a) experimental and (b) computational for $T/d = 3$ at $\mathrm{Re} = 750$.

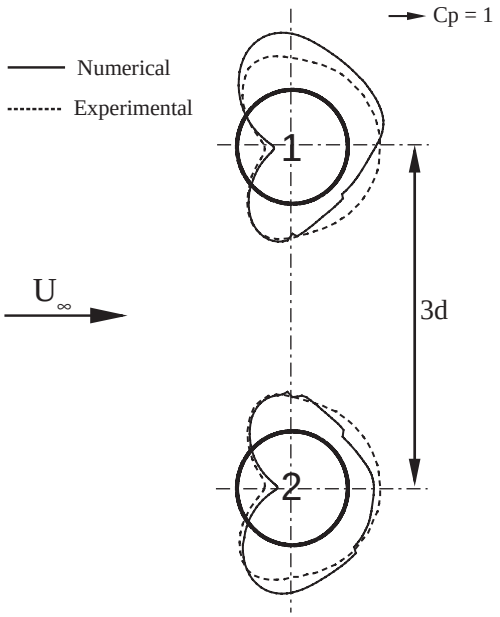

Fig. 5. Comparison of pressure distribution of $C_p = 1$ around each of the cylinders 1 and 2.

We compared our predictions against the specific experimental condition of Reynolds number of 750 and T/d ratio of 3. The predicted wake structures, as seen in Fig. 4, are in good qualitative agreement with the observed shedding vortices and the remarkable resemblance between the computational and experimental vortex streets, in terms of the symmetrical structure of two streets, is extremely encouraging. This phenomenological validation provided a degree of confidence in applying the LES model to adequately capture the complex turbulent flow characteristics of the wake formation. As the flow was perturbed passing over the side-by-side cylinders from the main stream, the generation of vortices behind the cylinders was found to be predominantly antiphase. Two distinct vortex streets propagated downstream. Another useful comparison between the LES prediction and experiment is the pressure distribution around the two cylinders, which can be seen in Fig. 5. The computed pressures also achieved good agreement with measurements.

The evolution of the transient wake vortex streets is depicted in Fig. 6. It was observed that the vortex structures for each of the streets were beginning to be detached to form closed loops downstream. As they acquired rounder shapes, these vortex structures were found to be similar to those of the Oseen vortices. Von Kármán postulated that at this large spacing of the side-by-side cylinders, it was impossible to maintain a stable gap vortex street. Our simulations indicated

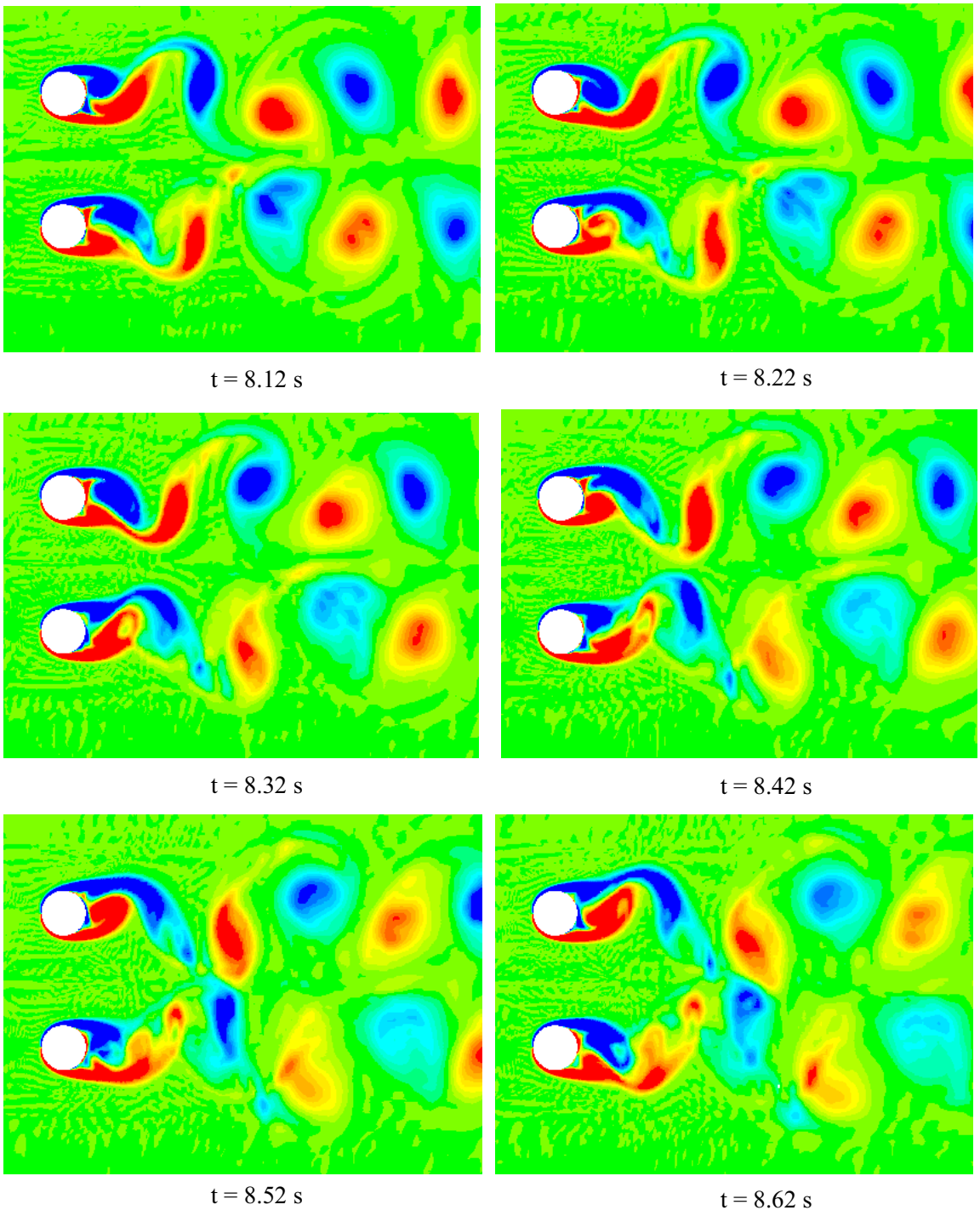

Fig. 6. Transient evolution of the asymmetrical wake streets—the contours of instantaneous spanwise vorticity between $|\omega_z| = 20$ (for $T/d = 3$ at Re = 750).

otherwise and since the gap vortices were sufficiently "far" apart, no squeeze and amalgamation of the vortex streets was observed. These two counter-rotating gap vortices were effectively self-adjusting to yield two stable vortex streets behind the two cylinders. This leads to a symmetrical pressure distribution around the cylinders resulting in the two

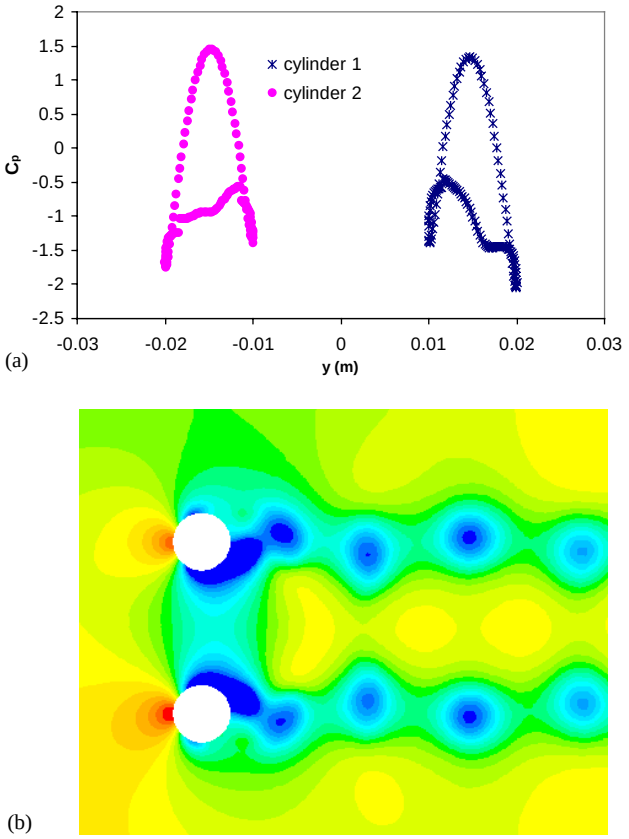

Fig. 7. Pressure distribution: (a) circumferential distribution of C_p and (b) pressure contours between -5 (blue) and $+5$ (red) at the middle plane for $T/d = 3$ at $\mathrm{Re} = 750$.

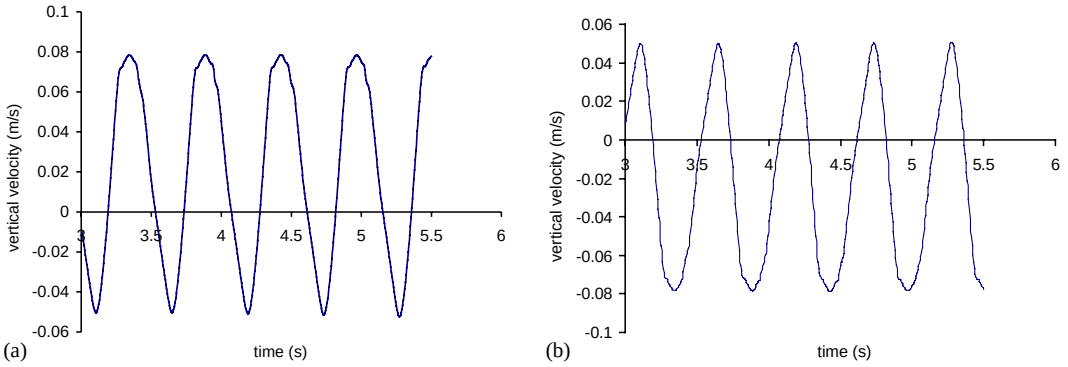

Fig. 8. Instantaneous vertical velocity as a function of time recorded at locations 1 and 2 (see Fig. 1(b)).

antiphase vortex streets. Fig. 7 illustrates the pressure distribution on the middle section of the two cylinder surfaces and pressure contours at the middle plane of the computational domain. It is clearly seen that a mirror-imaged pattern was predicted for the T/d ratio of 3. This finding was consistent with the generation mechanism of the two symmetrical vortex streets. The resultant lateral forces acting on the two cylinders were parallel, in close agreement with the experimental data of Zhou (2002). A small variation in pressure distribution on the trailing side of the cylinders was probably attributed to the wake turbulence (see Fig. 5). One important aspect worth noting is that the current numerical simulations could not predict any anti-asymmetrical vortex streets as observed through the experimental visualizations

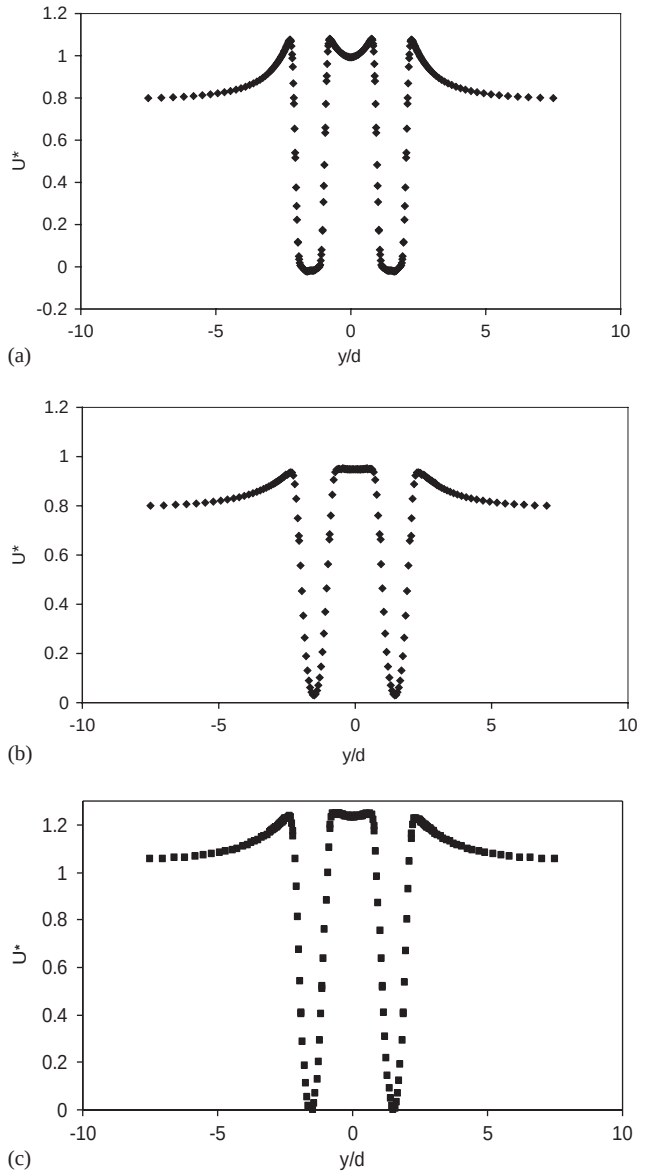

Fig. 9. Profiles of mean velocity: (a) computations at $x/d = 1.064$, (b) computations at $x/d = 1.5$ and (c) measurements at $x/d = 1.5$.

of Williamson (1985) and Zhou et al. (2001). They postulated that a small phase deviation from the antiphase mode between the gap vortices could lead to the formation of the in-phase vortex streets. In our simulations, we could not detect such occurrence. It might therefore suggest that the in-phase mode was the result of some external influence that was unable to be controlled during the experiments rather than an intrinsic behaviour of the flow. Fig. 8 demonstrates the temporal history of the vertical velocities calculated behind the cylinders at the horizontal distance $x/d = 1.5$ and vertical distances of $y/d = \pm 0.3$. The velocity spectrums revealed an out-of-phase periodic behaviour at an identical normalized frequency of 0.22. The mean velocity profiles in the near-wake region are given in Fig. 9. Interestingly, the streamwise mean velocity showed a gradual development from a U-shape profile at $x/d = 1.064$ (Fig. 9(a)) into a V-shape profile further downstream at $x/d = 1.5$ (Fig. 9(b)), which is caused by the transition to turbulence in the separating shear layer. We were unable to obtain any experimental data to compare this behaviour directly with the specific flow condition. We note the similarity in the structural dynamics of the near-wake flows over a range of Reynolds numbers between 300 and 300 000. By comparing our predicted velocities with a similarity solution for the

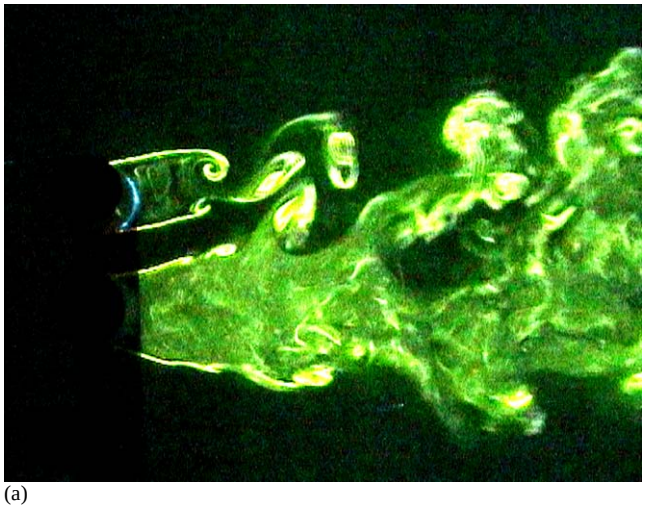

(a)

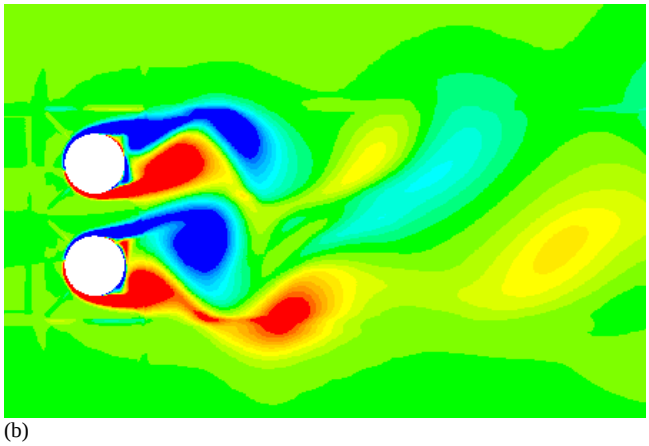

(b)

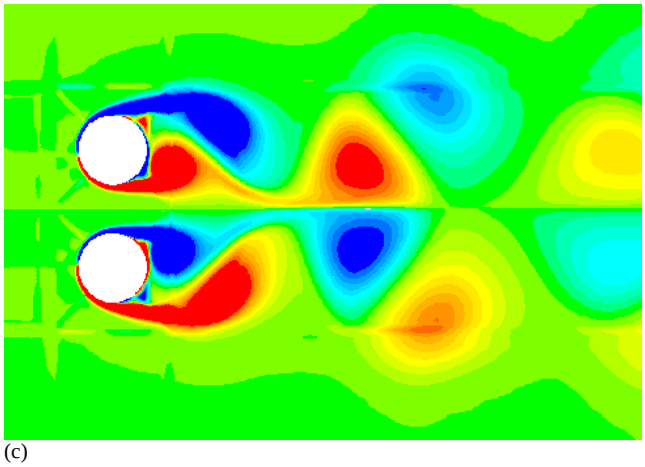

(c)

Fig. 10. Comparison of vortex structures—contours of instantaneous vorticity between $|\omega_z| = 20$ (red): (a) experimental, (b) computations with SGS model and (c) computations without SGS model for $T/d = 1.7$ at $\mathrm{Re} = 750$.

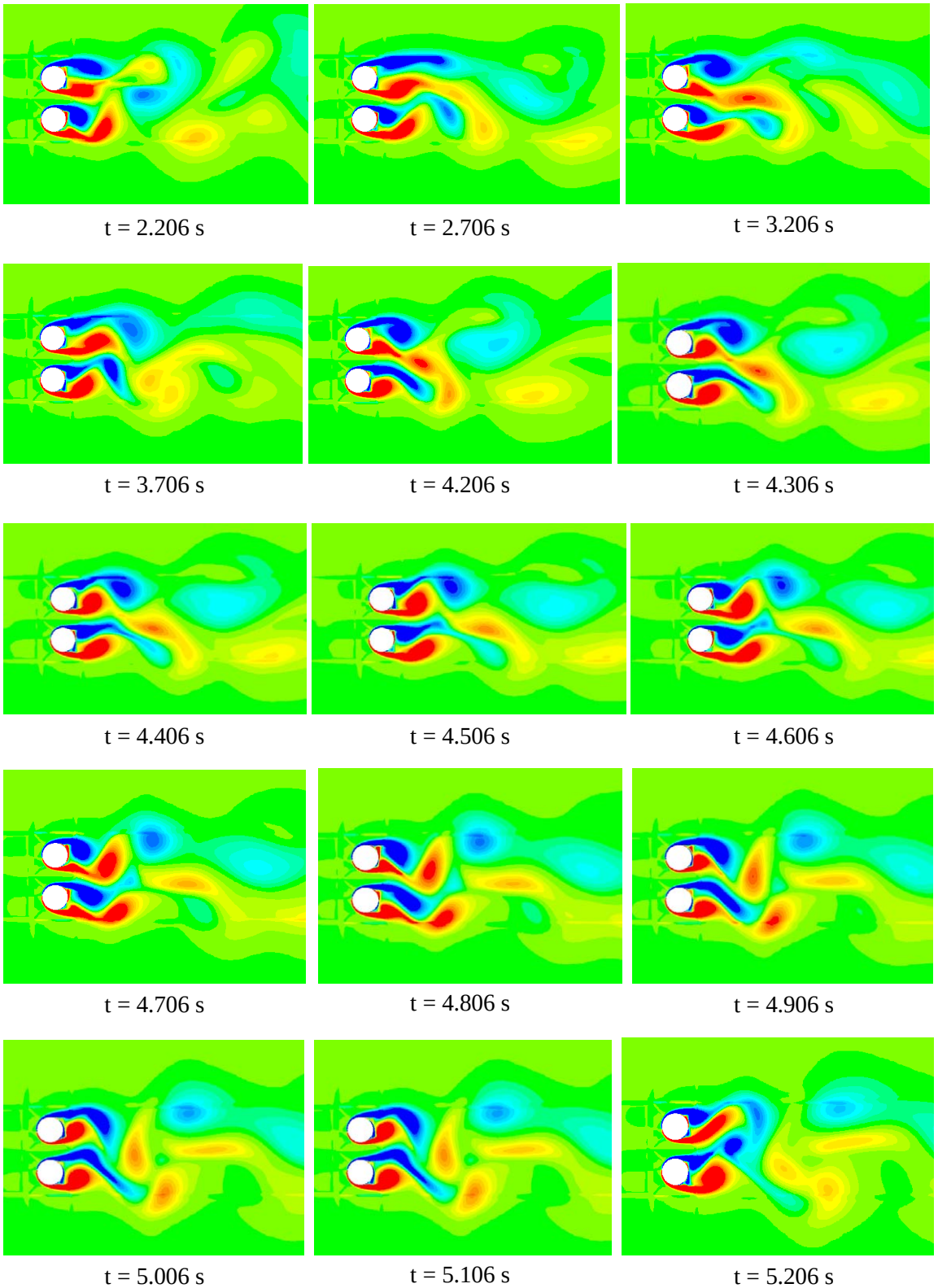

Fig. 11. Transient development of gap flow deflection followed by a large gap vortex shedding—the contours of instantaneous spanwise vorticities between $|\omega_z| = 20$.

conditions at Reynolds number of 3000 and x/d of 1.5, shown in Fig. 9(c), current predicted velocities were found to be under-predicted. We initially postulated that it might have been the result of inadequate resolution of the streamwise vortices. However, further mesh refinement study showed that was not the case. We believe that the discrepancy of our predictions on the separation shear layers could have been attributed to external experimental factors such as free-stream turbulence level (Bloor, 1964), acoustic noise (Cardell, 1993), cylinder vibrations (Prasad and Williamson, 1997) and end boundary conditions (Norberg, 1994) not accounted for in the model.

3.2. Stability of the gap flow deflection at intermediate cylinder spacing

Fig. 10 shows the predicted contours of instantaneous spanwise vorticity compared with laser-illuminated flow visualization experiments (Zhou, 2002) for Reynolds number of 750 and an intermediate transverse spacing T/d ratio of 1.7. The phenomenon is rather different from the aforementioned wake characteristics at T/d ratio of 3. It is observed that the gap flow between the two cylinders was deflected, forming one narrow wake from the top cylinder and one wide wake from the bottom cylinder. Two rows of vortices in the narrow wake appeared to be squeezed by pairing vortices rotating in opposite direction in the wide wake, which acted to absorb the approaching gap vortex, thus forming an amalgamated structure. The LES predictions of the wake structures for this configuration (see Fig. 10(b)) were also found to be in good qualitative agreement with the observed shedding vortices and once again the remarkable resemblance of the narrow and wide streets in terms of the characteristics of gap flow deflection between the computation and experiment was achieved. Fig. 10(c) presents the numerical simulation carried out without the use of a SGS model. It was evident that the absence of a SGS model significantly compromised the prediction of the gap flow deflection. It yielded a flow structure similar to that of the T/d ratio of 3—clearly a false representation of the wake structures actually observed during experiments.

The transient formation of the wake streets is illustrated in Fig. 11. The wake dynamics associated with the amalgamation and the squeezing effect of the gap vortices are clearly demonstrated. Here, the changeover of the deflected gap flow from one side to another is illustrated. Initially, the gap flow was deflected upwards. The vortices in the narrow wake from the top cylinder, as described above, tended to pair and absorb the gap vortex from the bottom cylinder. However, as time progressed, this large gap vortex in the wide wake collapsed, probably due to the strong interaction with the narrow wake. This consequently encouraged the growth of the gap vortex shed from the top cylinder. The large gap vortex in the narrow wake tended to prevent the merging of the following gap vortex shed from the bottom cylinder (wide wake). As a result, another large gap vortex was generated in the wide wake. This large gap vortex also quickly collapsed. Eventually, the large gap vortex from the top cylinder grew in strength and deflected the gap flow towards the bottom cylinder. At this intermediate spacing, a single vortex street was formed downstream instead of two distinct vortex streets observed in the large cylinder spacing of the preceding case. These transient simulations of the changeover characteristics of the deflected gap flow are in accordance with observations made in Zhou (2002).

To elucidate the occurrence of the gap flow deflection at intermediate cylinder spacing, we first examine the vertical velocity histories recorded at locations of 3 and 4 (see Fig. 1) in Fig. 12. Zhou et al. (2001) explained that the formation of the narrow wake was due to the gap vortex at the top cylinder travelling faster; possibly carried by the gap flow jet, which has a higher mean velocity. Our simulation clearly indicated that the deflection of the gap flow resulted from the frequency change in the velocities where the velocity of the top cylinder was shifted upwards with a constant amplitude from the bottom cylinder and this was in agreement with the experimental observations. We also note that the shedding time for the gap flow defection in our simulations (~ 5 s) was noticeably larger than the time scale of the Karman vortex

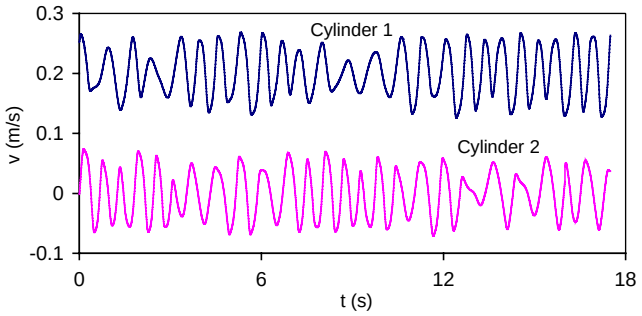

Fig. 12. Vertical velocity histories—cylinders 1 and 2—for $T/d = 1.7$ at $\mathrm{Re} = 750$.

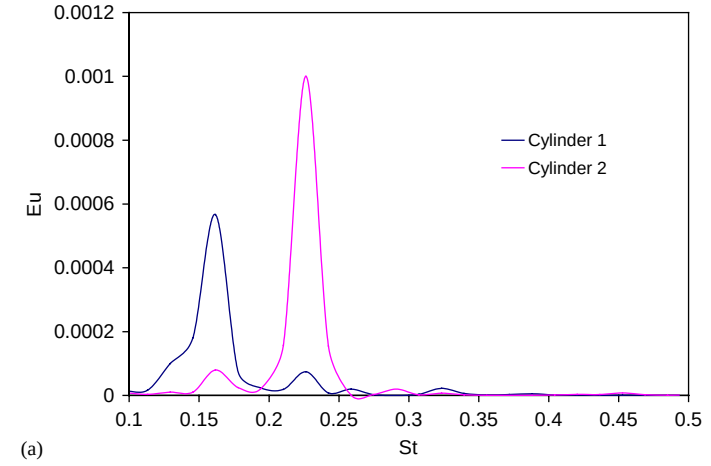

(a)

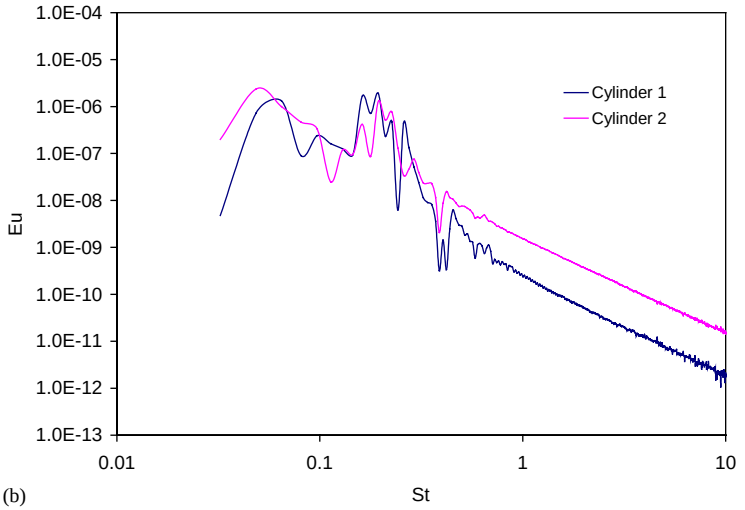

(b)

Fig. 13. Power spectrum of velocity fluctuations measured: (a) at locations 1 and 2 and (b) at locations 3 and 4 for $T/d = 1.7$ at $\mathrm{Re} = 750$.

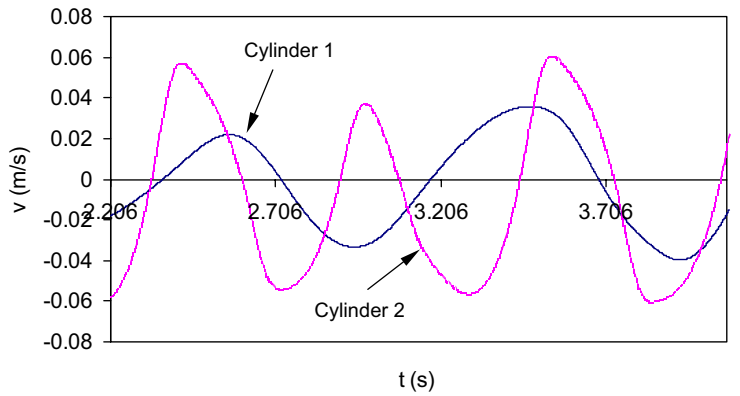

Fig. 14. Amalgamation of the vortexes and deflection of the gap flow indicated by the vertical velocities of cylinders 1 and 2.

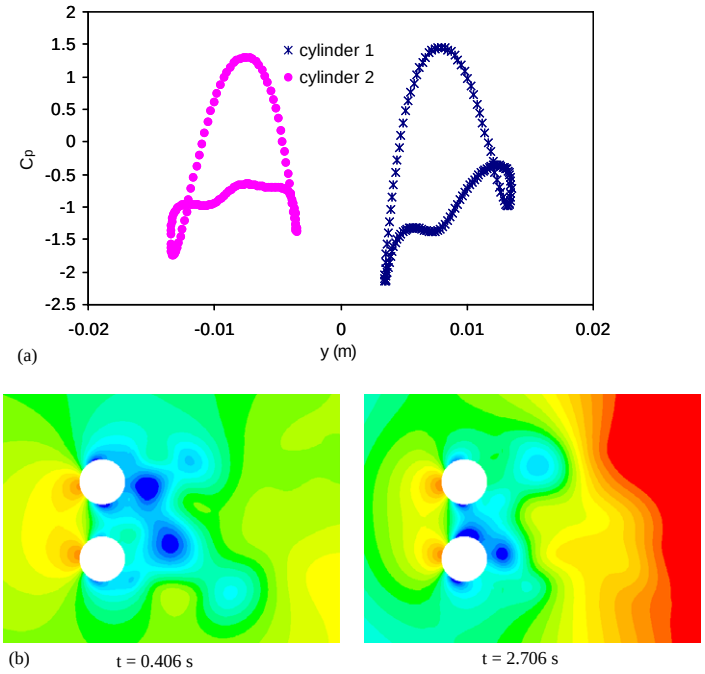

Fig. 15. Pressure distribution: (a) circumferential distribution of C_p and (b) pressure contours between -5 (blue) and $+5$ (red) at the middle plane at two different times for $T/d = 1.7$ at Re = 750.

shedding, but was much lower than the experimental observation by Kim and Durbin (1988). We are unsure whether this discrepancy has been caused by numerical noise or other unaccountable phenomenon in our simulations, which triggered the shear layer instability. Work is in progress to address this issue and findings on this matter will be reported in our future study.

Fig. 13 presents the relationship between the gap vortices and frequency with the profiles of the power spectrum of velocity fluctuation (Eu) against the Strouhal number ($\mathrm{St} = fd/U$). An amalgamation of the gap and outer vortices results in different frequency outputs at locations 1 and 2 (see Fig. 1(b)). Two different peak frequencies were observed. The narrow wake has a distinctly high Strouhal number while the wide wake has a low Strouhal number. The ratio of shedding frequencies was found to be about 1.5 (St equivalent to 0.16 and 0.24). Hot-wire measurements of Zhou (2002) gave a shedding frequency ratio of about 3. Measuring the correct shedding frequency at the precise location is a matter of constant debate. Fig. 13 demonstrates that the ratio of the shedding frequencies at locations 3 and 4 is different from the ratio determined at locations 1 and 2. This suggests that the shedding frequency has a high degree of variability in space and to ascertain the precise location where one should obtain the shedding frequency is extremely difficult either from simulations or experiments. Furthermore, we could not be certain that the experimental hot-wire measurements were free from errors and provided the correct shedding frequency at the precise location. We can argue that it is very plausible that in the narrow wake, given that the two lateral vortices were in very close proximity to each other, the hot-wire measurements (Zhou, 2002) may have detected a doubled frequency. In light of this aspect, the experimental shedding frequency is therefore half of the total measured value, which brings our predicted shedding frequency to be in accordance with the experimental value. Fig. 14 illustrates the amalgamated vertical velocity histories at downstream locations 1 and 2. Here, the out-of-phase vertical velocities were found prevalent between the top and bottom cylinders, highlighting the amalgamation and the squeezing effect of the vortices shedding behind the cylinders.

The pressure distribution around the cylinders, and pressure contours at the middle plane of the computational domains at two different times, are shown in Fig. 15. Unlike the symmetrical pressure distribution found for a T/d ratio of 3, a repulsive force acts on the cylinders within the intermediate spacing configuration, which is in accordance with the observations of Zhou (2002). For the transient pressure development, at the early time, the low-pressure distribution located near the top cylinder indicates the presence of the narrow wake with gap flow deflected upwards. At later time, the changeover of the gap flow was found deflected downwards towards the bottom cylinder as indicated by the low-pressure distribution (see Fig. 15(b)). It is also worth noting the formation of a large streak of vortices by the downstream high-pressure distribution.

4. Conclusion

The salient large-scale streamwise structures of the wake behind two side-by-side cylinders were simulated using the large-eddy simulation. Three-dimensional solution of the flow past the cylinders at Reynolds number of 750 was obtained. Calculations of the wake formation behind the cylinders were performed at two different T/d ratios. The following conclusions have been reached.

(i) For large cylinder spacing, $T/d = 3$, the numerical simulation confirmed the experimental observation of the formation of two symmetrical wake streets behind the cylinders. The symmetrical pressure distribution around the cylinders may have been responsible for the formation of the symmetrical vortex streets. Further downstream, the vortex structures from each of the streets began to be detached to form closed loops. As they acquired rounder shapes, these vortex structures were found to be similar to those of the Oseen vortices.

(ii) For an intermediate cylinder spacing, $T/d = 1.7$, the presence of gap flow deflection was predicted in accordance with experimental observations. Multiple peaks of shedding frequencies were obtained since the gap flow revealed a tendency to "flip" due to the gap squeezing effect and amalgamation of the vortices generated behind the cylinders. Current simulations predicted the ratio of shedding frequencies between the narrow and wide wakes to be 1.5. Although the hot-wire measurements yielded a value of 3, one plausible explanation is that in the narrow wake, given that the two lateral vortices were in very close proximity to each other, the measurements may have detected a doubled frequency. If this is the case, the shedding frequency predicted ratio comparable to the experimental value.

Acknowledgements

Some experimental results for comparison and valuable comments on this study provided by Dr. Y. Zhou at Hong Kong Polytechnic University are gratefully acknowledged.

References

Barkley, D., Henderson, R.D., 1996. Three-dimensional floquet stability analysis of the wake of a circular cylinder. Journal of Fluid Mechanics 322, 215–241.

Bearman, P.W., Wadcock, A.J., 1973. The interaction between a pair of circular cylinders normal to a stream. Journal of Fluid Mechanics 61, 499–511.

Bloor, M.S., 1964. The transition to turbulence in the wake of a circular cylinder. Journal of Fluid Mechanics 19, 290.

Boris, J., Grinstein, F., Oran, E., Kolbe, R., 1992. New insights into large-eddy simulation. Fluid Dynamic Research 10, 199–228.

Breuer, M., 1998. Large eddy simulation of the subcritical flow past a circular cylinder: numerical and modelling aspects. International Journal for Numerical Methods in Fluids 28, 1281–1302.

Cardell, G.S., 1993. Flow past a circular cylinder with a permeable splitter plate. Ph.D. Thesis, Graduate Aeronautical Laboratories, California Institute of Technology.

Goyder, H.G.D., 2002. Flow-induce vibration and noise in heat exchanger tube bundles. Proceedings of the 12th International Heat Transfer Conference, Grenoble, France.

Ishigai, S., Nishikawa, E., Nishmura, K., Cho, K., 1972. Experiment study on structure of gas flow in tube banks with tube axes normal to flow (Part I, Karman vortex flow around two tubes at various spacings). Bulletin of the JSME 15, 949–956.

Jones, W., 1994. Turbulence modelling and numerical solution methods for variable density and combusting flows. In: Libby, P.A., Williams, F.A. (Eds.), Turbulence Reactive Flows. Academic, Orlando, FL, pp. 309–374.

Jordan, S.A., Ragab, S.A., 1998. A large-eddy simulation of the near wake of a circular cylinder. ASME Journal of Fluids Engineering 120, 243–252.

Kim, H.J., Durbin, P.A., 1988. Investigation of the flow between a pair of cylinders in the flopping regime. Journal of Fluid Mechanics 196, 431–448.

Leonard, B., Mokhtari, S., 1990. Beyond first-order upwinding: the ultrasharp alternative for nonoscillatory steady-state simulation of convection. International Journal for Numerical Methods in Engineering 30, 729–766.

Liou, T.M., Wang, W.B., Chang, Y.J., 1995. Holographic interferometry study of spatially periodic heat transfer with ribs detached from one wall. Journal of Heat Transfer 117, 32–39.

Majumdar, S., Rodi, W., 1985. Numerical calculations of flow past circular cylinder. Proceedings of Third Symposium on Numerical and Physical Aspects of Aerodynamics. Long Beach, CA.

Meneghini, J.R., Saltara, F., Siqueira, C.L.R., Ferrari Jr., J.A., 2001. Numerical simulation of flow interference between two circular cylinders in tandem and side-by-side arrangement. Journal of Fluids and Structures 15, 327–350.

Mittal, R., Moin, P., 1997. Suitability of upwind-biased finite difference schemes for large eddy simulation of turbulent flows. AIAA Journal 35, 1415–1417.

Norberg, C., 1994. An experimental investigation of the flow around a circular cylinder: effect on controlled shear-layer vortices. Journal of Fluid Mechanics 258, 257.

Piomelli, U., Moin, P., Ferziger, J.H., 1988. Model consistency in large-eddy simulation of turbulent channel flows. Journal of Fluid Mechanics 162, 439–462.

Prasad, A., Williamson, C.H.K., 1996. The instability of the shear layer separating from a bluff body. Physics of Fluids A: Fluid Dynamics 8, 1347–1349.

Prasad, A., Williamson, C.H.K., 1997. The instability of the shear layer separating from a bluff body. Journal of Fluid Mechanics 333, 375.

Rodi, W., 1993. On the simulation of turbulent flow past bluff bodies. Journal of Wind Engineering and Industrial Aerodynamics 46–47, 3–19.

Rodi, W., Ferziger, J.H., Breuer, M., Pourquie, M., 1997. Status of large eddy simulation: results of a workshop. ASME Journal of Fluids Engineering 119, 248–262.

Scotti, A., Meneveau, C., Lilly, D.K., 1993. Generalized Smagorinsky model for anisotropic grids. Physics of Fluids A: Fluid Dynamics 5, 2306–2308.

Slaouti, A., Stansby, P.K., 1992. Flow around two circular cylinders by the random-vortex method. Journal of Fluid and Structures 6, 641–670.

Smagorinsky, J., 1963. General circulation experiment with the primitive equations: Part I. The basic experiment. Monthly Weather Review 91, 99–164.

Spivac, H.M., 1946. Vortex frequency and flow pattern in the wake of two parallel cylinders at varied spacings in steady cross-flow. Journal of Aeronautical Sciences 13, 289–297.

Sumner, D., Price, S.J., Paidoussis, M.P., 1998. Investigation of side-by-side circular cylinders in steady cross-flow by particle image velocimetry. In: Bearman P.W., Williamson, H.K. (Eds.), Proceedings 1988 ASME Fluids Engineering Division Summer Meeting, Paper 37.

Tutar, M., Holdø, A.E., 2000. Large eddy simulation on a smooth circular cylinder oscillating normal to a uniform flow. ASME Journal of Fluids Engineering 122, 694–702.

Tutar, M., Holdø, A.E., Lewis, A.P., 1998. Comparative performance of various two equation models and LES on simulated flow past a circular cylinder in subcritical flow regime. Proceedings of ASME Fluids Engineering Summer Meeting on Finite Element Application in Fluid Dynamics, Washington, DC, USA.

Williamson, C.H.K., 1985. Evolution of a single wake behind a pair of bluff bodies. Journal of Fluid Mechanics 159, 1–18.

Williamson, C.H.K., 1996. Vortex dynamics in the cylinder wake. Annual Review of Fluid Mechanics 28, 477–539.

Xu, S.J., Zhou, Y., So, R.M.C., 2003. Reynolds number effects on the flow structure behind two side-by-side cylinders. Physics of Fluids 15, 1214–1219.

Zdravkovich, M.M., 1977. Review of flow interference between circular cylinders in various arrangements. Journal of Fluids Engineering 99, 618–633.

Zdravkovich, M.M., 1987. The effects of interference between two circular cylinders in cross flow. Journal of Fluids and Structures 1, 239–261.

Zhou, Y., 2002. Private communication.

Zhou, Y., Wang, Z.J., So, R.M.C., Xu, S.J., Jin, W., 2001. Free vibrations of two side-by-side cylinders in a cross flow. Journal of Fluid Mechanics 443, 197–229.